PATTERNS OF DAMAGE IN IGNEOUS AND SEDIMENTARY ROCKS UNDER CONDITIONS SIMULATING SEA-SALT WEATHERING

C. CARDELL,[1] T. RIVAS,[2]* M.J. MOSQUERA,[3] J.M. BIRGINIE,[4] A. MOROPOULOU,[5] B. PRIETO,[2] B. SILVA[2]
AND R. VAN GRIEKEN

[1] *Department of Chemistry, University of Antwerp (UIA), Universiteitsplein 1, B-2610 Antwerp, Belgium*
[2] *Department of Soil Science, University of Santiago de Compostela, 15706 Santiago de Compostela, Spain*
[3] *Department of Physical Chemistry, Faculty of Science, University of Cádiz, Puerto Real, Cádiz, 11510, Spain*
[4] *Laboratory of Civil and Maritime Construction – IUT, 15 rue Vaux de Foletier, 17026 La Rochelle, France*
[5] *Department of Chemical Engineering, Laboratory of Materials Science and Engineering, National Technical University of Athens, 9 Iroon Polytechniou Street, Zografou Campus, Athens, Greece*

ABSTRACT

A saline-spray artificial ageing test was used to simulate the effects produced in granites and sedimentary rocks (calcarenites, micrites and breccia) under conditions in coastal environments. Three main points were addressed in this study: the durability of the different kinds of rock to salt decay, the resulting weathering forms and the rock properties involved in the weathering processes. For this, mineralogical and textural characterization of each of the different rocks was carried out before and after the test. The soluble salt content at different depths from the exposed surfaces was also determined. Two different weathering mechanisms were observed in the granite and calcareous rocks. Physical processes were involved in the weathering of granite samples, whereas dissolution of calcite was also involved in the deterioration of the calcareous rocks. We also showed that microstructural characteristics (e.g. pore size distribution), play a key role in salt damage, because of their influence on saline solution transport and on the pressures developed within rocks during crystallization. Copyright © 2003 John Wiley & Sons, Ltd.

KEY WORDS: sea-salt weathering; ageing tests; pore structure; granitic rocks; calcareous rocks

INTRODUCTION

Soluble salts are recognized as being important weathering agents in dry environments and in coastal areas (Evans, 1969). In coastal areas, the development of certain weathering morphologies (sand disaggregation, honeycomb, tafoni) is attributed to the action of marine salts, and the role of sodium chloride has been widely emphasized (Mustoe, 1982; Bradley *et al.*, 1978; Robert *et al.*, 1996). These geomorphological features, which can be spectacular in natural environments, may, however, cause serious problems when they appear in material used for building in coastal areas, especially very porous sedimentary rocks (Rossi Manaresi and Tucci, 1989; Rivas, 1997). Most of the techniques for investigating these types of weathering morphologies have therefore been developed by groups interested in the conservation of stone-built national heritage monuments. Studies of the effect of soluble salts on the types of rock from which these monuments are built provide a reference point for analysis of these types of weathering and have been extremely useful in establishing the mechanisms involved (Bromblet *et al.*, 1996; Casal *et al.*, 1989; Silva-Hermo *et al.*, 1996).

In this field of study, artificial weathering tests are generally applied to investigate the weathering mechanisms whereby soluble salts cause weathering, and to compare the decay processes of different rock materials under identical conditions. Standard procedures for artificial weathering tests have been elaborated by several international organizations such as RILEM, ASTM (USA), DIN (Germany), NORMAL (Italy) and UNE (Sweden).

---

* Correspondence to: T. Rivas, Department of Soil Science, University of Santiago de Compostela, 15706 Santiago de Compostela, Spain. E-mail: edtere@usc.es

These simple testing routines are very useful for establishing the relative resistance of different types of rock and the durability of conservation treatments. However, because of the need to reduce the number of factors that produce weathering and to increase their intensity in order to obtain results in a short time, the tests are sometimes oversimplified. This makes it difficult to establish the weathering mechanisms under natural conditions.

A number of researchers have developed other procedures aimed at realistically reproducing environmental conditions in an attempt to understand the synergistic action of decay factors affecting rocks under natural conditions. Among these, the procedure based on Auger (1988) and applied in Rivas *et al.* (2000a,b) and Birginie *et al.* (2000) has allowed the types of weathering associated with marine salts found in natural environments to be successfully reproduced in the laboratory. The factors determining these good results are the use of sea water instead of pure solutions and the environmental conditions established in the design of these procedures.

In the present study, we have applied the latter procedure to calcareous and granitic rocks, in order to compare the weathering morphologies developed in each type of rock and to evaluate the changes in texture and mineralogical composition produced under certain conditions. Finally, this investigation leads us to establish which are the intrinsic parameters of stones that are implicated in the weathering process. Because microstructural parameters play a major role in salt deterioration (McGreevy, 1996; Rodriguez-Navarro and Doehne, 1999; Theoulakis and Moropoulou, 1997), special attention has been paid to evaluation of the pore structures of the different types of rocks. Microstructure obviously plays a key role in water transport kinetics in porous networks, and is also important in determining the pressures associated with crystallization (Mosquera *et al.*, 2000).

MATERIAL AND METHODS

Rock material

Three different granites from Galicia (NW Spain) and seven different types of calcareous rock from Apulia (S Italy) were chosen for study. These rocks were chosen because of their importance in the construction of buildings and monuments in the areas mentioned. Macroscopic and microscopic characterization of each of the rocks is briefly described below.

For the artificial ageing test, prisms of $5 \times 5 \times 7$ cm were cut from all of the types of rock. A reference plane was taken during the cutting of test prisms so that all prisms were oriented in the same way. The sedimentary plane was taken as the reference plane for calcareous rocks, whereas for granites it was the bedding plane of the quarry.

Granites. Three migmatitic granites known as Muros (M), Roan (R) and Barbadelo (B) were selected for study. Muros is a medium- to fine-grained, two-mica anatexic granite with an inequigranular anhedral texture and slight orientation of its mineral components. The main components are quartz, plagioclase, microcline, muscovite (which marks the orientation of the rock) and biotite, with zircon, turmaline, apatite and magnetite as accessory minerals. Microscopy reveals a fissural system characterized by inter- and transgranular fissures, the latter with a clear orientation.

Roan is a medium- to fine-grained two-mica granite with a panallotriomorphic equigranular texture, signs of flow structure and containing xenoliths. It is a fairly homogeneous granite with no apparent orientation. Fissuring is slight, mainly consisting of inter- and intragranular fissures. Intragranular fissures mainly affect feldspars ($c.$ 9·7 μm) associated with the many inclusions existing in these minerals, e.g. plagioclases (associated with sericitization) and micas (muscovite and biotite); intergranular fissures are mainly between quartz grains.

Barbadelo is a medium- to fine-grained, two-mica granite with an inequigranular allotriomorphic texture, mineral orientation marked by biotites, and Fe-oxy-hydroxide segregation. Its main components are quartz, potassium feldspar, plagioclase (slightly sericitized), biotite (partially chloritized), muscovite and, as the main accessory, apatite. This granite shows the highest degree of fissuring; fissures are intra- and transgranular, the latter showing marked orientation.

Calcareous rocks. The following calcareous rocks from Apulia (Italy) were selected for the study: the limestone referred to as CNR3 is from Salerno and those referred to as MSA1, SMLA, SMLB, SMLC, SMLD and SMLE are from Gargano.

CNR3 and MSA1 are coarse-grained homogeneous limestones composed of sparytic calcite (grain size >10 μm). Both also contain quartz and micas; fossil bryozoans are also observed in CNR3. These rocks have a high intergranular porosity with well-connected pores. SMLA is a brecciate limestone composed of big sparry calcite crystals, and it has very high intra- and intergranular porosity. Rims of calcite crystals of different dimensions (ranging between 20 and 100 μm) form growths on the margins of the pores towards their centres, resulting in the so-called 'drusy mosaic'.

The SMLB, SMLC, SMLD and SMLE rocks are very homogeneous biomicrites with fossils well cemented with micrite (grain size <5 μm). In the SMLB micrite, a few foraminifers are observed, in the SMLC, bryozoans are very abundant, SMLD contains bryozoans and algae, and in SMLE some foraminifers were observed. Stylolites filled with sparry calcite are present in SMLB, SMLC and SMLE rocks. The porosities observed under petrographic microscopy of SMLB, SMLC and SMLD are lower than that of SMLE; in the latter, the porosity is concentrated mainly in the stylolites.

Salt-spray ageing test

Five test prisms of each rock were subjected to an ageing test using a controlled atmosphere chamber. This chamber, described in Auger (1988) and Birginie *et al.* (2000) is electronically programmed to produce cycles of 1 min of saline spray followed by 29 min of drying by forced air at 35–39 °C and 50 per cent relative humidity. The saline spray is produced by passing a constant flow of air through a capillary tube supplied with sea water (the composition of which is shown in Table I), connected to a standardized spray-gun.

The test prisms were placed on a revolving stand, which makes four complete turns during spraying of the salt solution so that all samples were exposed to similar amounts of the solution (0·4 g per sample). The granites and the coarse limestones were subjected to this test during 70 days (3360 cycles) and the micrites during 140 days (6720 cycles).

Although previously published information (Smith and McGreevy, 1988) helped in the choice of drying temperature and type of solution, the choice was finally determined by the results of tests carried out with these and other types of rocks, generally based on the recommendations of RILEM, ICR-CNR. From these tests, it has been concluded that the type of salt (sulphates, nitrates, chlorides), the nature of the solution (mixed or pure) and the drying temperature have a strong influence on the type of weathering produced in calcareous rocks (Cardell, 1998) and granites (Rivas *et al.*, 2000b). Thus, it has been demonstrated that the uptake of solutions by capillary action, the use of pure solutions of sodium chloride and drying temperatures of between 40 and 60 °C, far from reproducing natural conditions, may produce effects not seen in natural environments. These results are the reason for the use of sea water and a fixed drying temperature of less than 40 °C. The time of the drying and spraying periods and the intensity of spraying were selected from those found, during various tests of the system, to allow a medium to low degree of weathering to be reproduced in a short time.

Techniques for monitoring the modifications induced by the test

The following methods and analytical techniques were used to evaluate the modifications induced by the test.

Table I. Sea-salt composition (expressed in ppm) used in the artificial ageing test

Cl^-	SO_4^{2-}	NO_3^-	PO_4^{3-}	Mg^{2+}	Ca^{2+}	Na^+	K^+
22 050	2713	50	28	945	345	19 920	1020

Salinity (S ‰) = 39·20; chlorinity (Cl ‰) = 21·70 (Mohr test); conductivity (C) = 33 s cm^{-1}.

Visual evaluation of decay. Samples were observed in a stereomicroscope and a description of the weathering forms developed was made following the terminology proposed by Delgado Rodrigues (1991).

X-ray diffraction (XRD). This technique was applied in order to determine the mineralogical composition of the rocks, and was carried out before and after the test.

Petrographic microscopy. This was used to describe the changes in the pore system as well as the texture and mineral composition of the rocks, in depth from the exposed surfaces. For this, thin sections were prepared from fragments cut parallel to each prismatic plane of the test prisms before and after the test. The pore system in the granites (which is mainly a fissural system) was described more precisely using *fluorescence microscopy*, adding a fluorescent dye (rhodamine B) to the plastic resin in order to visualize the types of fissures and their orientation.

Scanning electron microscopy. A scanning electron microscope equipped with an energy dispersive X-ray detection system was used to study mineralogical modifications and the nature and habits of crystallized salts after the test. For this, samples were broken perpendicularly to the exposed surfaces of the test prisms, and were later carbon coated.

Soluble salt analysis. Chloride, nitrate, sulphate, calcium, sodium, magnesium and potassium contents of the test prisms and their distribution at depth from the exposed surfaces were analysed using the following procedure. Powder samples were extracted from one of the four sides of the prisms by drilling into the samples in successive steps. Two holes were drilled on the same side of the prisms, at 2·5 cm from the borders and with approximately 2 cm between the two boreholes. Samples were taken at each of five successive stages of 5 mm to a depth of 25 mm. Stages of 3 mm were used in the Roan granite in order to check the salt concentration profile more precisely. About 100 mg of powder was dispersed in 100 ml of distilled water and placed in an ultrasonic bath for 25 min. The anions in the filtered aqueous suspensions were measured by ion chromatography (IC) and the cations by inductively coupled plasma-atomic emission spectroscopy (ICP-AES).

Mercury intrusion porosimetry (MIP). This was used to analyse the microstructural changes in the rock samples. The MIP measurements were carried out with both a low- and high-pressure porosimeter, thus allowing pressures of between 10^{-4} and 300 MPa to be developed. This enabled pore radii of between 2·5 nm and 58 mm to be measured. In calcareous rocks, samples extracted from the surface of the exposed prisms were compared with samples taken from the interior of the prisms and with samples not subjected to the test. For all the MIP analyses, 2 cm^3 fragments extracted from the test prisms and previously cleaned in a microwave and dried at 60 °C were used.

RESULTS

Granites

Macroscopic inspection of the samples at the end of the test revealed that some of the granites were more deteriorated than some of the calcareous rocks, e.g. the micrites. In all the granites, small, hard and cohesive scales were developed; also, to a lesser extent, pitting was developed in plagioclases. The intensity of the scaling was directly proportional to the total porosity (Table II), therefore Barbadelo was the most deteriorated granite followed by Muros and Roan, which showed a similar degree of deterioration.

The semi-quantitative results of the XRD analysis (Table III) revealed traces of vermiculite and kaolinite, indicating that even before the test, the granites were no longer completely fresh. The pre-Hercynian origin of the samples and the fact that they have suffered tectonic processes means that they had developed many fissures in the quarry and this had favoured weathering and therefore neoformation of secondary minerals such as kaolinite or vermiculite. However, there was no increase in the amount of secondary minerals in samples after being subjected to the test, indicating that the deterioration factors did not cause detectable changes in geochemistry or mineral composition.

Examination, by fluorescence microscopy, of thin sections of specimens subjected to the test revealed that this has induced the formation of transgranular fissures running parallel to the exposed faces of the test prisms of all three granites. These transgranular fissures ran to depths of 600 μm in the Muros granite and to a depth of 500 μm in Barbadelo granite. In Roan granite these fissures did not run as deep as in other granites (400 μm). Interestingly, in the Muros and Barbadelo samples the pre-existing transgranular fissures

Table II. Pore system of the granites before and after the salt crystallization test

Granites	T_P (%)	Pores in each radius range			Macrofissures	Microfissures
		60–3·3 μm	3·3–0·1 μm	<0·1 μm	(μm (%))	(μm (%))
Muros*	3·9	30·52	51·42	18·06	60–5·9 (27·3)	4·4–0·01 (72·7)
Muros	4·5	49·73	28·77	21·90	60–4·4 (49·3)	$3·3–2·4 \times 10^{-3}$ (50·67)
Roan*	2·1	31·72	59·75	8·53	60–1·8 (42·7)	0·6–0·03 (57·3)
Roan	5·9	31·46	36·28	32·27	60–1·8 (50·8)	$1–2·4 \times 10^{-3}$ (49·2)
Barbadelo*	4·9	46·37	42·97	10·66	60–1·8 (61·7)	$1·8–7·8 \times 10^{-3}$ (38·3)
Barbadelo	6·4	54·13	24·03	21·84	60–1·3 (64·6)	$1·3–2·4 \times 10^{-3}$ (35·4)

T_P, total porosity
* Results before salt crystallization test.

Table III. Semi-quantitative analysis, by X-ray diffraction, of the granites before the test

	Q	F	M	K	V
Muros	++	++	++	Tr	–
Roan	++	++	++	Tr	Tr
Barbadelo	++	++	*	Tr	–

Q, quartz; F, feldspars; M, micas; K, kaolinite; V, vermiculite
++, >50%; +, 50–30%; *, 30–10%; Tr, <3%; –, not detected.

(visualized before the test) run parallel to one of the two prismatic planes (and thus, perpendicular to the second prismatic plane). Microscopic visualization of the thin sections at the end of the test revealed that the transgranular fissures always developed parallel to the exposed surfaces, even when the pre-existing fissures were perpendicular to these surfaces (Figure 1).

The SEM study showed that the main differences in granite samples before and after the test were the presence of salts (i.e. halite, gypsum and Mg-sulphate) and a higher fissuration degree after the test. There were no signs of chemical weathering in the granites, other than those already present before the test. In the Muros granite, isolated acicular crystals of gypsum, either growing from cubic crystals of halite (Figure 2a) or covering halite layers, were visualized. The Roan granite contained fewer salts; only some acicular crystals of gypsum and isometric crystals of halite were identified. The Barbadelo granite developed the greatest number of fissures and tabular crystals of gypsum (*c.* 100 μm) and thin layers of halite spread all around its surface were found (Figure 2b).

The ion concentrations of aqueous extracts of samples taken at different depths from the exposed surfaces of the granites are shown in Figure 3. Similar profiles were observed for the three granites, and in all cases, the amounts of salts were attributed to the test. The highest ion concentrations were detected in the first 5 mm from the sample surfaces, and then rapidly decreased towards the interior. The main ions present were Na^+ and Cl^-. The similar amounts of these ions suggest the presence of halite (confirmed by SEM-EDX). Also present in the following decreasing order were: SO_4^{2-}, Ca^{2+}, Mg^{2+} and K^+; NO_3^- was not detected. The significant amounts of SO_4^{2-} and Ca^{2+} in the first 5 mm in Muros and Barbadelo granites are consistent with the presence of gypsum, revealed by SEM. The Muros and Barbadelo granites contained similar amounts of solubilized ions and the Roan granite contained the lowest amounts.

The results of total porosity and the pore radius distribution obtained by MIP are summarized in Table II. As previously shown (Mosquera *et al.*, 2000), the pore radius distribution was clearly bimodal in all granites, with the first linear segment of the intrusion curve corresponding to macrofissures and the second to microfissures. Comparing the results of MIP and fluorescence microscopy (Figure 1), we concluded that macro-fissures corresponded to transgranular fissures, and microfissures to inter- and intragranular fissures. In order to
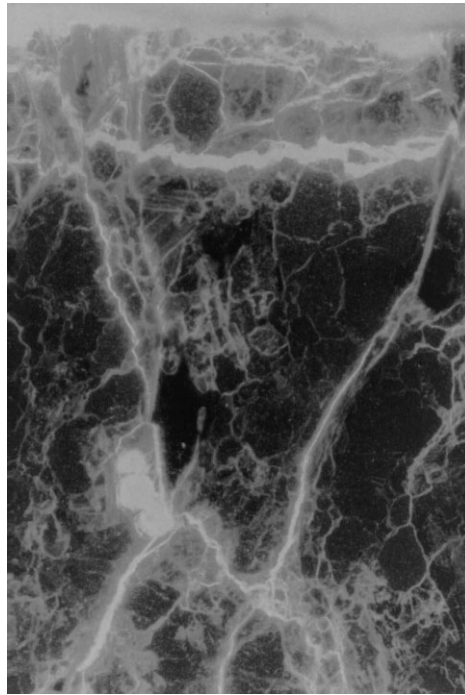
Figure 1. Microphotograph, taken using fluorescence microscopy, of fissures running sub-parallel to the surface of Muros granite, at the end of the artificial ageing test (5×)
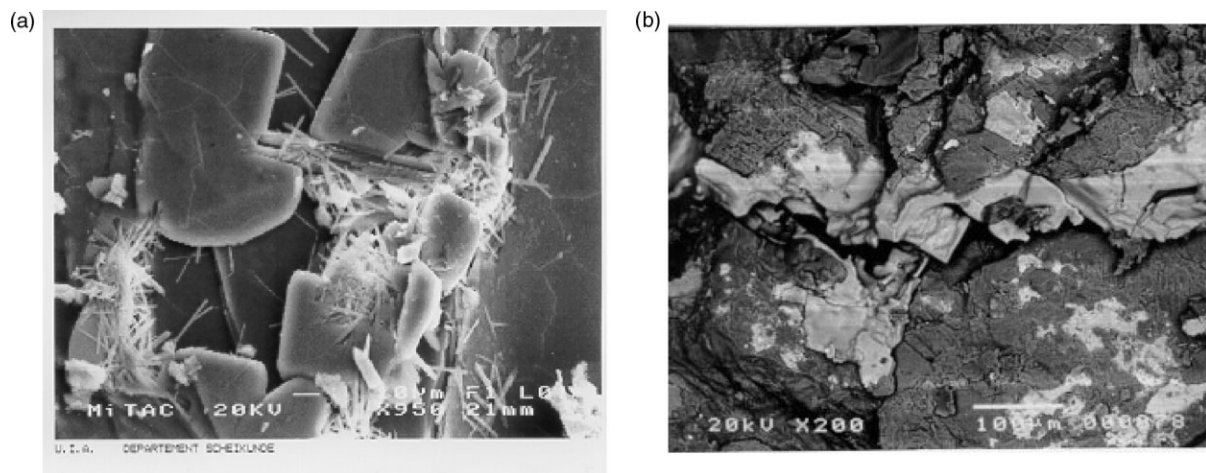

Figure 2. (a) SEM microphotograph of halite cubes and needle-shaped whiskers of gypsum crystallized at the surface of Muros granite at the end of the artificial ageing test. (b) SEM microphotograph showing the crystallization of a halite layer in the fissures of Barbadelo granite at the end of the artificial ageing test

compare the results, the pores were divided into three size ranges: range **a** (3·3–60 μm); range **b** (0·1–3·3 μm) and range **c** ($2·4 \times 10^{-3}$–0·1 μm). The range of macro- and microfissure radii was also noted (the percentage of each is shown in parentheses in Table II).

Before the test, the distribution of fissures showed clear differences between the granites. The minimum radius of the macrofissures in the Muros granite was 6 μm whereas in Barbadelo and Roan granites it was much
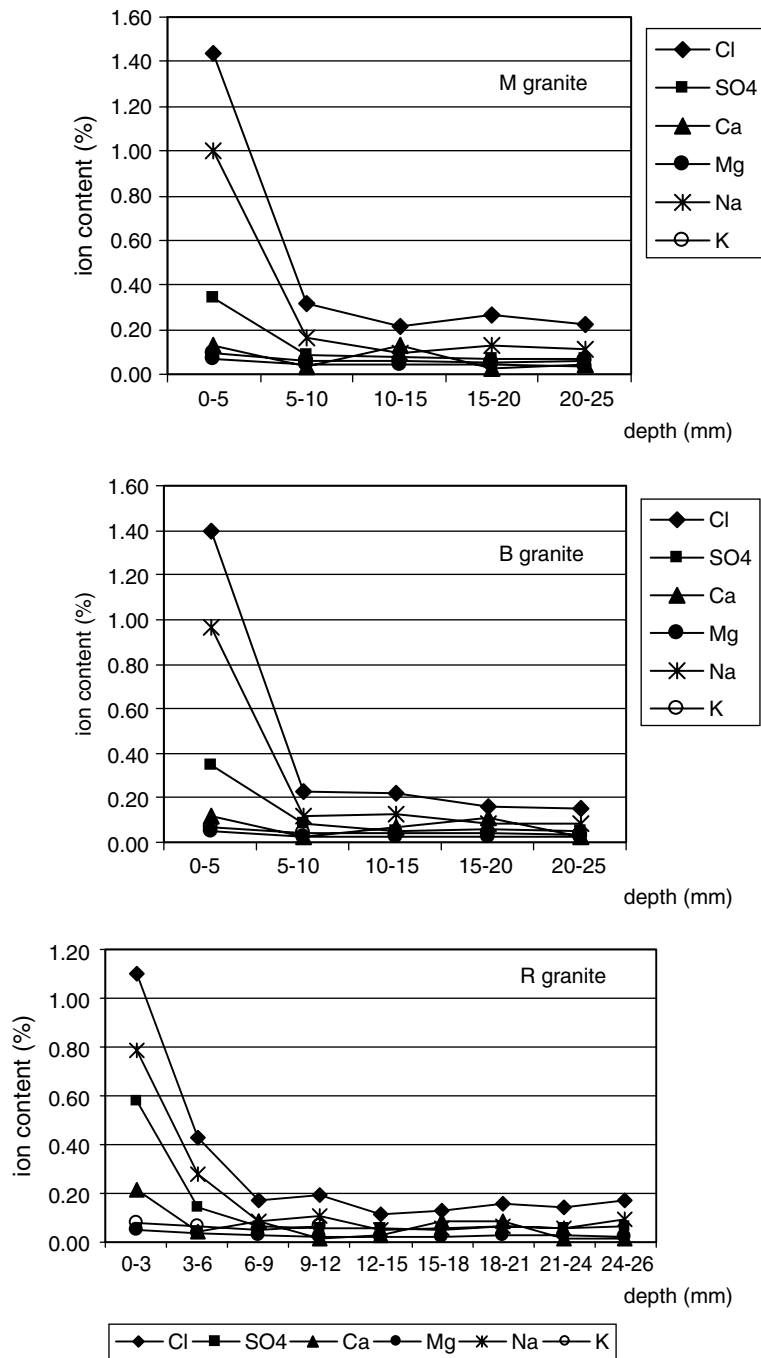
Figure 3. Soluble salt content of extracts corresponding to the surface and deeper layers (0–5 mm) of the three granites subjected to the artificial ageing test. Values are expressed as percentages

smaller (1·8 μm). Moreover, the proportion of macrofissures was significantly different in each rock: from 27 per cent for Muros to 62 per cent for Barbadelo. Similar differences were observed for the microfissures.

After the test, the porosity increased by 0·6 per cent in the Muros granite. There was an increase in the number of pores with radii in range **a** (the largest) and a decrease in the number in range **b**. The artificial

test also led to an increase in the proportion of macrofissures (from 27 to 49 per cent) and a decrease in the minimum radius of macrofissures from 5·9 to 4·4 µm. The proportion of microfissures decreased to a greater extent (from 72 to 50 per cent) and a new group of micropores with radii smaller than the minimum radius found in sound specimens (10 nm) was also observed.

The total porosity of Roan granite subjected to the test increased by around 3 per cent, the percentage of pores in the 3·3−60 µm radius size range remained constant, while in the 0·1−3·3 µm range it decreased and in the $0·1−2·4 \times 10^{-3}$ µm range it increased considerably (from 8·5 to 32 per cent). A new group of microfissures with radii below the minimum size found in quarried samples (30 nm for this granite) was also found. The proportion of macrofissures increased in samples subjected to the test while the minimum radius remained constant.

In Barbadelo, there was an increase in total porosity, after the test, of 1·5 percentage points. The percentage of pores within the radius size range 3·3−60 µm increased, those in the range 0·1−3·3 µm decreased and those in the range $2·4 \times 10^{-3}$−0·1 µm doubled (due to the presence of micropores with radii less than 0·01 µm). In this sample there was a slight increase in the percentage of macrofissures and a decrease in the minimum radius (from 1·8 to 1·4 µm).

Calcareous rocks

Macroscopic inspection of the calcareous rock samples after the test showed that the coarse-grained limestones CNR3 and MSA1 were more weathered than the micrites. The CNR3 limestone developed slight scaling and erosion of the edges as decay forms, and MSA1 showed incipient signs of scaling and marked Fe-oxide stains. The brecciate limestone SMLA showed less deterioration than the other limestones, and displayed slight granular disaggregation and efflorescences. The micrites SMLB, SMLC, SMLD and SMLE (the least porous, Table IV) remained virtually unchanged. Only SMLB showed slight granular disintegration at the edges and in the stylolites.

Analysis by X-ray diffraction revealed the mineralogical composition of the calcareous rocks before and after the test to be fairly similar. Calcite was the only mineral detected, except in the decayed coarse-grained limestones (CNR3 and MSA1) in which halite, not present before the test, was also identified.

Observations made by petrographic microscopy showed that the test conditions caused changes in the texture and mineral composition of the samples. Following the test, the coarse-grained limestones CNR3 and MSA1 and the micrite SMLA showed evidence of calcitic cement dissolution. In the SMLB micrite, there was some evidence of sparite dissolution in the stylolites. In the SMLC, SMLD and SMLE micrites, isolated fissures developed parallel to the surface (Figure 4a) and efflorescences covered the surface of SMLD (Figure 4b).

The SEM study showed the presence of halite cubes filling the smallest pores in the brecciate limestone (SMLA). Halite was also identified as a homogeneous thin layer covering the surface of the SMLD micrite (Figure 5). Chlorine was detected in the rest of the micrites, and sulphur in the SMLC and SMLE samples. A non-continuous, very thin carbonate crust covered the surface of the SMLA, SMLC and SMLE micrites.

The distribution of the different dissolved ions at depth from the weathered surfaces is shown in Figure 6. We observed both qualitative and quantitative differences among the different limestones. In the coarse-grained limestones (CNR3 and MSA1), the soluble salt contents were much higher than in the breccia SMLA or in the micrites; the latter contained very small amounts, even less than the granites.

The main ions present in CNR3 and MSA1 were Na^+ and Cl^-; in the breccia SMLA there were also similar amounts of SO_4^{2-}. The ion content was high in the first 5 mm then decreased sharply except in the MSA1 limestone where the highest salt concentration was detected at a depth of 5−10 mm from the surface. The main ions present in the SMLB, SMLC, SMLD and SMLE micrites were also Na^+ and Cl^- along with Ca^{2+}. As in the other limestones, the levels of Na^+ and Cl^- decreased with depth. However, the levels of Ca^{2+} remained fairly constant at depth. This may indicate that calcium carbonate was dissolved during extraction.

The results of the MIP analysis of the calcareous rocks before and after the test are shown in Table IV. In the coarse-grained limestones, CNR3 and MSA1, which are the most porous limestones, the test produced a slight decrease in porosity (from 36 to 33 per cent) in the former and a slight increase (from 27 to 30 per cent) in the latter. In both of these rocks, the variation in porosity was similar at the surface and at depth.

Table IV. Pore system of the calcareous rocks before and after the salt crystallization test

	T_P (%)	Pore size distribution (% of pore volume)				
		<0·1 μm	0·1–0·5 μm	0·5–1·0 μm	1·0–5·0 μm	5·0–60 μm
CNR3*	36·3	10·20	46·48	13·97	22·69	6·66
CNR3[a]	33·6	8·92	48·75	13·32	25·83	3·18
CNR3[b]	34·0	9·14	52·03	15·58	21·93	1·32
MSA1*	27·4	1·39	7·82	6·76	38·73	45·31
MSA1[a]	30·0	0·17	14·49	12·43	29·61	43·30
MSA1[b]	31·4	0·29	10·05	10·05	24·73	54·88
SMLA*	6·89	37·68	50·72	2·46	3·04	6·09
SMLA[a]	7·50	8·67	6·67	3·87	23·47	57·33
SMLA[b]	7·75	4·90	3·99	3·22	18·43	69·46
SMLB*	5·47	19·38	7·86	5·48	17·18	50·09
SMLB[a]	1·63	49·08	4·29	0·61	2·45	43·56
SMLB[b]	3·73	32·89	0·00	0·00	1·07	66·04
SMLC*	0·22	–	–	–	–	–
SMLC[a]	0·83	–	–	–	–	–
SMLC[b]	0·60	–	–	–	–	–
SMLD*	0·22	21·74	30·43	13·04	30·43	4·35
SMLD[a]	2·24	23·66	0·00	0·00	0·00	76·34
SMLD[b]	1·39	39·42	0·00	7·30	14·60	38·69
SMLE*	2·79	–	–	–	–	–
SMLE[a]	1·47	–	–	–	–	–
SMLE[b]	2·82	–	–	–	–	–

T_p, total porosity.
* Results before salt crystallization test.
[a] Samples from the surface of the rocks.
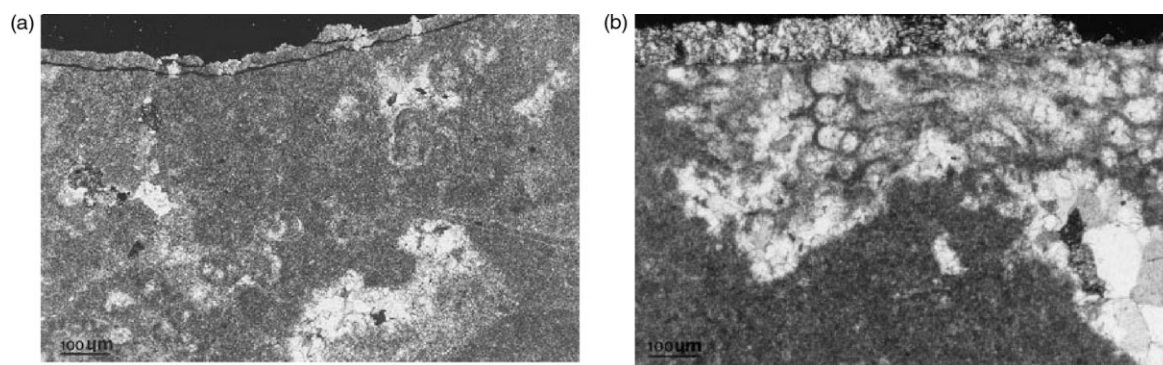[b] Samples from the interior of the rocks.
– , Not determined.

Figure 4. (a) Microphotograph taken with petrographic microscopy illustrating the isolated microfissures parallel to the surface of SMLC micritic limestone at the end of the artificial ageing test. Crossed nicols. (b) Microphotograph, taken with petrographic microscopy, illustrating the halite efflorescences crystallized at the surface of SMLD micritic limestone, at the end of the artificial ageing test. Also, detail of moldic porous results from the removal (usually by solution) of an individual constituent of a rock, such as a shell. Here the porous of a bryozoan are filled with secondary $CaCO_3$. Crossed nicols

Examination of the pore size distribution showed that in CRN3 there was a slight increase in the number of pores with radii >5 μm and also pores with radii <0·1 μm at the end of the test. In MSA1, there was a decrease in the percentage number of pores with radii <0·1 μm and an increase in the percentage of pores with radii in the range 0·1–1 μm.
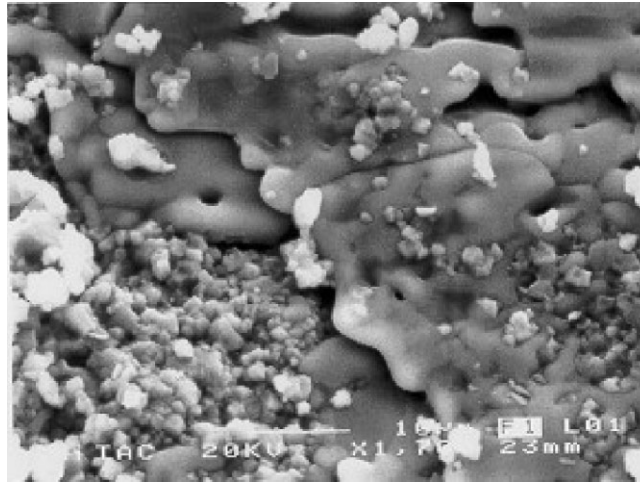
Figure 5. SEM microphotograph of a continuous and thin halite crust coating the surface of the SMLD micritic limestone

The total porosity of the breccia (SMLA) (6·8 per cent) increased slightly after the test both close to and beneath the surface. Nonetheless, the pore size distribution changed dramatically: the percentage of pores with radii <0·5 μm decreased and the percentage of pores with radii >1 μm increased.

Regarding the micrites, the porosity at the end of the test of SMLC and SMLD had increased (especially in areas close to the surface), and the porosity of SMLB and SMLE had decreased (also most notably in the area closest to the surface). The distribution of pore radius size was only able to be determined for SMLB and SMLD. In SMLB (in which there was a decrease in porosity), there was a decrease in the number of pores with radii of intermediate size (0·1–5 μm) and a large increase in the number of pores with small radii (<0·1 μm). In SMLD almost the opposite was found, i.e. a decrease in the percentage number of pores with radii of intermediate size (0·1–5 μm) and a large increase in the number of pores with radii >5 μm.

DISCUSSION

The types of weathering developed during the test were, in granites, very small scales, and in calcareous rocks both granular disintegration and scaling. In both types of rocks the weathering was attributed to the action of the saline solution used in the test. This conclusion was also reached in previous studies (Rivas *et al*., 2000; Birginie *et al*., 2000) in which these and other rocks were subjected to the same test.

Microstructural analysis and study of thin sections of the granite samples clearly showed that scaling was caused purely by the physical processes of salt crystallization and dissolution (there were no changes in geochemistry or mineralogical composition). This weathering form (scaling) was reported in granitic rocks situated in coastal areas; in these situations, this form is characterized by the presence of Na and Cl (as the main ions) but also sulphate ions (Silva-Hermo *et al*., 1996). In the present test, the main salt precipitated was sodium chloride and to a lesser extent calcium and sodium sulphates. These salts crystallize in pre-existing fissures and exert pressures greater than the resistance of the material, thereby causing new fissures (such as those observed by microscopy to run parallel to the surface) and an increase in porosity. The MIP analysis revealed an increase in the proportion of macrofissures (consistent with the findings of the analysis of thin sections), a decrease in the minimum radius of macrofissures and microfissures and thus an increase in the proportion of pores with a smaller radius. The latter was attributed to the pores being covered by crystals of sodium chloride or sodium sulphate.

The susceptibility of the granites to weathering was determined by three factors: firstly, the porosity, which affects the ease of entry of saline solution and by implication the amounts of salts within the rock; secondly, the grain size–medium- to coarse-grained granites are more susceptible to salt decay (Silva-Hermo *et al*.,
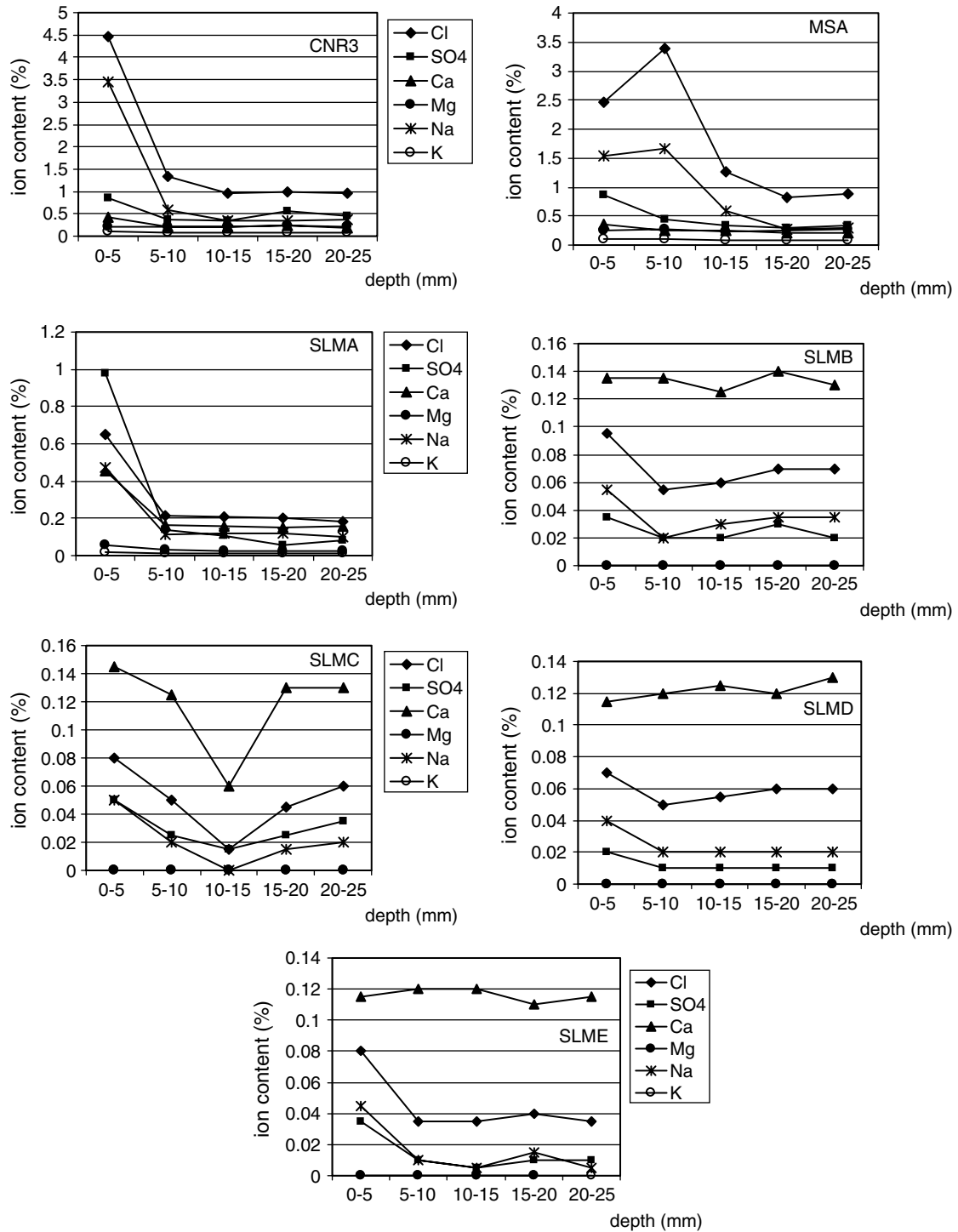
Figure 6. Soluble salt content of extracts corresponding to the surface and deeper layers (0–5 mm) of the limestones subjected to the artificial ageing test. Values are expressed as percentages

1996); finally, the pore system, which to a large extent determines the crystallization pressure that the salt exerts and therefore the deterioration produced. Crystallization pressure can be defined by the equation:

$$p = \frac{2\gamma}{r} \tag{1}$$

where γ is interfacial tension of salt solution and r is the rock pore radius. Crystallization pressure is therefore inversely proportional to the pore radius. Thus, the pressure exerted by salt crystallization in small pores is greater than in larger pores and is more likely to overcome the resistance of the material (Rossi-Manaresi and Tucci, 1989; Fitzner and Snethlage, 1982; Benavente *et al.*, 1999).

Furthermore, saline spray transport in a rock pore system mainly occurs via laminar viscous flow. The vapour flux q is given by Darcy's law:

$$q = k\frac{A\Delta p}{\eta l} \tag{2}$$

where k is the specific permeability, A is the cross-section, Δp is the pressure gradient, η is the vapour viscosity and l is the thickness of the specimen. If the pore system is considered as a set of parallel tubes, k is given by:

$$k = \frac{\varepsilon r^2}{8} \tag{3}$$

where ε is the porosity and r is the radius of the tube.

Following these equations, the vapour flux of a saline solution (and therefore the amount of salt that enters the rock) is governed by the specific permeability, which in turn is governed by the porosity and pore radius of the rock.

Therefore in small pores in granitic rocks (corresponding to inter- and intragranular fissures) water vapour transport is slow, and water, which is taken up by macrofissures, is then retained in the microfissures where, according to Equation 1, crystallization pressure occurs, favouring the formation of fissures. Small pores in the Roan, Muros and Barbadelo granites are those in the size range <3·3 μm, accounting for 70 and 57 per cent of all the pores in the less porous granites such as Muros and Roan.

Interpretation of some of the results obtained with the limestones is complicated because, as well as the physical disruption caused by salt crystallization, the calcareous cement dissolves, sometimes leading to the formation of a subsurface crust. We attribute the dissolution of the carbonated cement to the action of the saline solution. Birginie *et al.* (2000) have shown that if the sea water in the artificial ageing test is replaced by distilled water, no weathering occurs in limestones and, more significantly, the pore system is not altered. We thus conclude that the dissolution of the cement is associated with the greater ionic strength of the saline solution used (compared with that of distilled water), which therefore increases the dissolving power of water. This does not occur in granites: the processes involved in the natural weathering of granite in the presence of water are different from those involved in limestone weathering – hydrolysis takes place in the former, leading to the formation of secondary minerals. The fact that the amount of these minerals did not increase during the test indicates that the only weathering processes that took place were crystallization and dissolution of soluble salts.

The different forms of weathering observed in the limestones were therefore caused by salt crystallization and dissolution of the cement. Sand disaggregation is caused by the salt crystallization through the same physical process described for the granites (i.e. crystallization pressure exerted into the pore system). The dissolution of the cement and its precipitation in areas close to the evaporation surface probably cause the formation of a crust, which differs from the rest of the rock in terms of porosity. The physico-mechanical characteristics in the surface area are therefore modified and in turn the evaporation rate of the salt solution is affected. The crystallization of salt below the crust can cause the formation of fissures parallel to it and eventually, detachment of the crust. However, some authors suggest that the crust may avoid further

deterioration in the underlying stone, because it acts as a dense hard skin at the surface (Delalieux *et al.*, 2001; Maravelaki-Kalaitzaki and Biscontin, 1999).

Because salt crystallization and cement dissolution occur together, it is impossible to study them separately; some of the results, especially those of the MIP analysis, are therefore difficult to interpret.

In some calcareous stones, the MIP results are easily interpreted despite the complexity of the processes that take place in these rocks compared with those in granites. In the SMLC and SMLD limestones, in which fissures formed parallel to the surface, there was an increase in porosity, particularly in areas close to the surface, and at the same time in SMLD there was an increase in the number of pores with radii >5 μm. However, salt crystallization may also act in another way, causing a decrease in porosity due to pores being covered by salt crystals. This appears to be the reason why in SMLE, which showed the least amount of weathering and deposition of efflorescences, there was a decrease in total porosity close to the surface.

However, in those cases in which cement dissolution was produced (MSA1, SMLA, SMLB and CNR3 limestones), it is difficult to establish the relationship between this process and the changes in porosity and pore size distribution, because there may be an increase in porosity in those areas where the cement dissolves and a decrease in porosity where it recrystallizes.

Regarding the susceptibility of the limestones to the weathering process, the smaller the pore size, the higher the pressures caused by salt crystallization, therefore it was expected that CNR3 and SMLA would be the most severely weathered following the test (they have the highest percentages of pores with small radii). However, this did not occur and CNR3 and MSA1 (the coarse-grained limestones) were the most severely weathered. These were the most porous of the limestones and it appears that, as with the granites, the greater porosity allowed more solution to enter the rocks (the most porous rocks contained the highest levels of soluble salts). In these highly porous limestones, the uptake of the solution favoured by their high total porosity ($27-36$ per cent) enhanced saline solution absorption. In addition, a high percentage of pores had radii <5 μm, which implies greater crystallization pressure and therefore greater deterioration. This reasoning based on the percentage of small-sized pores also appears to explain the greater deterioration of the breccia (SMLA) compared with the micrite (SMLB), which had similar porosities. The percentage of pores with radii <5 μm in SMLP was 49 per cent and in SMLA, 93·91 per cent. In the other micrites, the very low total porosities ($0·2-2·0$ per cent), the interlocking texture and the pore system built up by small isolated pores, do not favour the access and transport of salt solutions towards the interior and evaporation takes place at or just below the surface. In the former case, efflorescences precipitate causing an aesthetic effect (SMLD). In the latter case, the salt crystallization pressures induced the formation of isolated microfissures (SMLC, SMLD and SMLE). In spite of these weathering characteristics, the resistance of the micrites suggests that their mechanical strength was not compromised. The response of the micrites to the salt crystallization test was also favoured by their well aggregated fine-grained calcitic cement.

CONCLUSIONS

From the results, we drew the following conclusions.

The weathering produced in granite and limestone rocks was due exclusively to the effect of the sea water solution, either by disruption caused by salt crystallization (mainly sodium chloride and sodium sulphate) or by dissolution of the calcareous cement in the limestones.

In the granites, weathering was produced exclusively by the pressure exerted by salts crystallizing within pre-existing fissures. In these rocks the total porosity, grain size and the percentage of microfissures present (inter- and intragranular fissures) determined the susceptibility to weathering because of their effect on transport of the saline solution and the pressure exerted by salt crystallization.

In the limestones, the effect of the calcareous cement dissolution was added to the effect caused by the pressure exerted by salt crystallization. In these rocks, total porosity (undoubtedly affected by the grain size of the cement and the degree of aggregation) appeared to determine the degree of weathering; for the same total porosity, the percentage of pores with small radii may increase the susceptibility to weathering.

The usefulness of the artificial ageing test for reproducing the weathering that takes place in coastal areas was once again demonstrated.

REFERENCES

Auger F. 1988. Simulation accélérée de la dégradation des matériaux de construction en ambiance aérienne saline. In *IAEG Conference on the Engineering Geology of Ancient Works, Monument and Historical Sites*, Marinos PG, Koukis GC (eds). Balkema: Rotterdam; 797–804.

Benavente D, Del Cura MA, Fort R, Ordóñez S. 1999. Thermodynamic modelling of changes induced by SALT pressure crystallization in porous media of stone. *Journal of Crystal Growth* 168–178.

Birginie JM, Rivas T, Prieto B. 2000. Comparaison de l'altérabilité au brouillard salin de deux pierres calcaires au moyen des mesures pondérales, acoustiques et par traitement d'imagines. *Materiales de Construcción* **50**(259): 27–43.

Bradley WC, Hutton JT, Twidale CR. 1978. Role of salts in developments of granitic tafoni, south Australia. *Journal of Geology* **86**: 647–654.

Bromblet P, Bernabe E, Verges-Belmin V. 1996. Petrophysical investigations on the origin of scaling of a microgranular magmatic rock associated to granite in the monuments from Brittany (France). In *Report n°5 on Degradation and Conservation of Granitic Rocks in Monuments. Protection and Conservation of European Cultural Heritage*, Vicente MA, Delgado-Rodrigues J, Acevedo J (eds). European Commission: Brussels; 73–78.

Cardell C. 1998. *Cristalización de sales en calcarenitas: aplicación al Monasterio de San Jerónimo*. Doctoral Thesis, Department of Mineralogy and Petrology, University of Canada.

Casal M, Silva B, Delgado J. 1989. Agents and forms of weathering in granitic rocks used in monuments. In *Proceedings of European Symposium on Science, Technology and European Cultural Heritage*, Bologna Baer NS, Sabbioni C, Sors DI (eds). Commission of European Communities, 439–442.

Delalieux F, Cardell-Fernández C, Tudorov V, Dekov V, Van Grieken R. 2001. Environmental conditions controlling the chemical weathering of the 'Madara Horseman' Monument, NE Bulgaria. *Journal of Cultural Heritage* **2**: 43–54.

Delgado Rodrigues J. 1991. Proposal for a terminology of stone decay forms on monuments. *News Letter Group of Petrography of the ICOMOS Stone Committee* 2–4.

Evans IS. 1969. Salt crystallization and rock weathering: a review. *Revue de géomorphologie dynamique* **XIX**(4): 153–177.

Fitzner B, Snethlage R. 1982. Ueber Zusammenhange zwischen Salzkristallisationsdruck und Poreradienverteilung. *nin G.P. Newsletter* **3**: 13–24.

Maravelaki-Kalaitzaki P, Biscontin G. 1999. Origin, characteristics and morphology of weathering crust on Istria stone in Venice. *Atmospheric Environment* **33**: 1699–1709.

McGreevy JP. 1996. Pore properties of limestone as controls on salt weathering susceptibility: a case study. *Processes of Urban Stone Decay* **13**: 150–167.

Mosquera MJ, Rivas T, Prieto B, Silva B. 2000. Capillary rise in granitic rocks: interpretation of kinetics on the basis of pore structure. *Journal of Colloid and Interface Science* **222**: 41–45.

Mustoe GE. 1982. Origin of honeycomb weathering. *Geological Society of America Bulletin* **93**: 108–115.

Rivas T. 1997. *Mecanismos de alteración de rocas graníticas utilizadas en la construcción de monumentos antiguos en Galicia*. Doctoral Thesis, Servicio de Publicaciones e Intercambio Científico. Universidad de Santiago.

Rivas T, Prieto B, Silva B, Birgine JM, Auger F. 2000a. Comparison between traditional and chamber accelerated ageing tests on granitic rocks. *Proceedings of Ninth International Congress on Deterioration and Conservation of Stone*, Venice (Italy). 171–180.

Rivas T, Prieto B, Silva B, Birginie JM. 2000b. Granite decay by marine salt-spray accelerated ageing test. In *Protection and Conservation of the Cultural Heritage of the Mediterranean Cities*, Galán E, Zezza F (eds). A. A. Balkema: Rotterdam; 227–231.

Robert M, Bernabe E, Bromblet P, Jaunet AM, Verges-Belmin V, Penven MJ. 1996. Identification of two alteration microsystems chemical and physical, causing granite and kersantite degradation in Brittany (France). In *Report n°5 on Degradation and Conservation of Granitic Rocks in Monuments. Protection and Conservation of European Cultural Heritage*, Vicente MA, Delgado-Rodrigues J, Acevedo J (eds). European Commission: Brussels; 67–71.

Rodriguez-Navarro C, Doehne E. 1999. Salt weathering: influence of evaporite rate, supersaturation and crystallisation pattern. *Earth Surface Processes and Landforms* **23**(3): 191–209.

Rossi-Manaresi R, Tucci A. 1989. Pore structure and salt crystallisation: "salt decay" of Agrigento biocalcarenite and "case hardening" in sandstone. In *I International Symposium on Conservation of Monuments in the Mediterranean Basin*, Bari, Zezza F (ed). Grafo: Bresica, Italy; 97–100.

Silva-Hermo B, Rivas-Brea T, Prieto-Lamas B. 1996. Relation between type of soluble salt and decay forms in granitic coastal churches in Galicia (NW Spain). In *Report n°4: Origin, Mechanism and Effects of Salts on Degradation of Monuments in Marine and Continental Environments*, Zezza F (ed). University C.U.M. School: Bari, Italy; 181–190.

Smith BJ, McGreevy JP. 1988. Contour scaling of a sandstone by salt weathering under simulated hot desert conditions. *Earth Surface Processes and Landforms* **13**: 697–705.

Theoulakis P, Moropoulou A. 1997. Microstructural and mechanical parameters determining the susceptibility of porous building stones to salt decay. *Journal of Construction and Building Materials* **11**(1): 65–71.